Noname manuscript No.
(will be inserted by the editor)

A Positivity-preserving High Order Finite Volume Compact-WENO Scheme for Compressible Euler Equations

Yan Guo · **Tao Xiong** · **YuFeng Shi**

arXiv:1402.5618v1 [math.NA] 23 Feb 2014

Received: date / Accepted: date

Abstract In this paper, a positivity-preserving fifth-order finite volume compact-WENO scheme is proposed for solving compressible Euler equations. As we know conservative compact finite volume schemes have high resolution properties while WENO (Weighted Essentially Non-Oscillatory) schemes are essentially non-oscillatory near flow discontinuities. We extend the main idea of WENO schemes to some classical compact finite volume schemes [32], where lower order compact stencils are combined with WENO nonlinear weights to get a higher order finite volume compact-WENO scheme. The newly developed positivity-preserving limiter [46, 44] is used to preserve positive density and internal energy for compressible Euler equations of fluid dynamics. The HLLC (Harten, Lax, and van Leer with Contact) approximate Riemann solver [39, 2] is used to get the numerical flux at the cell interfaces. Numerical tests are presented to demonstrate the high-order accuracy, positivity-preserving, high-resolution and robustness of the proposed scheme.

Keywords Compact scheme · finite volume · weighted essentially non-oscillatory scheme · positivity-preserving · compressible Euler equations

1 Introduction

Computing numerical solutions of nonlinear hyperbolic systems of conservation laws is an interesting and challenging work. In recent years, a variety of high resolution schemes which are of high order accurate for smooth solutions and non-oscillatory for discontinuous

Yan Guo
Department of Mathematics, China University of Mining and Technology, Xuzhou, Jiangsu 221116, P.R. China.
E-mail: yanguo@cumt.edu.cn

Tao Xiong
Department of Mathematics, University of Houston, Houston, Texas 77004, U.S.A.
E-mail: txiong@math.uh.edu

YuFeng Shi
School of Electric Power Engineering, China University of Mining and Technology, Xuzhou, Jiangsu 221116, P.R. China.
E-mail: shiyufeng@cumt.edu.cn

solutions without introducing spurious oscillations have been proposed for these problems. WENO schemes [25,17,35,36] have high order accuracy in smooth region and keep the essentially non-oscillatory properties for capturing shocks. However, these classical WENO schemes often suffer from poor spectral resolution and excessive numerical dissipation.

Compact schemes [22] have attracted a lot of attention due to its spectral-like resolution properties by using global grids. These schemes have the features of high-order accuracy with smaller stencils and easier application of boundary conditions. However, linear compact schemes necessarily produce Gibbs-like oscillations around shock waves when they are applied directly to flow with discontinuities, and the amplitude does not decrease with mesh refinement. In recent years, there are a variety of methods trying to overcome this problem. A hybrid compact-ENO scheme for shock-turbulence interaction problem is proposed in [1], where compact scheme is coupled with an ENO scheme near discontinuities. A similar hybrid scheme which coupling a fifth-order compact upwind algorithm in a conservative form with WENO scheme is proposed in [32] for shock-turbulence interactions. This conservative hybrid compact-WENO Scheme is proven to have better resolution properties than standard WENO schemes and hybrid compact-ENO schemes. Ren et. al. [33] have proposed a new hybrid scheme as the weighted average of the conservative compact scheme [32] and the WENO scheme by using a smoothness indicator, the resulting hybrid scheme switches to essentially non-oscillatory scheme near the flow discontinuities. In [34], Shen et. al. have proposed a compact scheme, in which the discontinuity is treated as an internal boundary. These hybrid schemes require indicators to detect discontinuities and switch to a non-compact scheme around discontinuities, thus spectral-like resolution properties would be lost. Another methodology for capturing discontinuities has been proposed by Deng et. al. [6]. They have developed nonlinear compact schemes, where adaptive compact stencils are used. Deng and Zhang [7] also have proposed weighted compact nonlinear schemes (WCNS) based on the weighted technique. As extensions of [6], Zhang et. al. [43] propose to directly interpolate the flux by using the Lax-Friedrichs flux splitting and characteristic-wise projections. An improvement of the schemes [7,43] converging to the steady-state solution of Euler equations has been studies in [42]. More nodes than a standard compact scheme are used to form the schemes in [6,7,43], so that the compactness of these schemes are lost. Along this line, a new linear central compact scheme was proposed in [26] based on [22], both grid points and half grid points are used to get higher order accuracy and better resolution. According to the idea of the WENO schemes, Jiang et. al. [18] have proposed weighted compact schemes where the final compact scheme is a weighted combination of compact substencils. By using the two biased third order compact stencils and a central fourth order compact stencil, they can get a sixth order central compact scheme in smooth regions. Ghosh et. al. have employed the idea in [18], and developed a class of compact-reconstruction finite difference WENO schemes [11], where lower order compact stencils are identified at each interface and combined with nonlinear WENO weights. Upwind compact schemes can be obtained by using the biased compact interpolations.

The compact methods described above are based on finite difference approach. However, In order to satisfy the governing laws of the fluid physics, finite volume approach which are inherently conservative are usually adopted. In recent years, very few papers dealing with compact schemes are based on finite volume method in literature. Gaitonde et. al. have proposed compact-difference-based finite-volume schemes for linear wave phenomena in [10]. Kobayashi extends Gaitonde's work and has proposed a class of Padé finite volume methods for linear equations in [19]. Piller et. al have developed compact finite-volume schemes based on staggered grids for numerical simulation of collinear Navier-Stokes equations in [30]. In [31], Piller et. al. have proposed another high-order compact finite volume method

for the scalar advection-diffusion equation, where advective fluxes are computed by the compact scheme introduced in [32] and the diffusive fluxes are discretized by using the Padé methods [19]. In [20], Lacor et. al. have proposed a finite volume formulation of compact central schemes on arbitrary structured grids, where the fluxes are obtained by using compact interpolation of values on cell interfaces in the physical space. In the present work, we will construct a new high-order compact scheme based on a finite volume approach for compressible Euler equations.

In this paper, we consider the compressible Euler equations. The conservative formulation of the Euler equations is given by

$$U_t + F(U)_x = 0, \tag{1.1}$$

where U and $F(U)$ are vectors of conserved variables and fluxes respectively, which are given by

$$U = \begin{bmatrix} u_1 \\ u_2 \\ u_3 \end{bmatrix} = \begin{bmatrix} \rho \\ \rho u \\ E \end{bmatrix}, F(U) = \begin{bmatrix} \rho u \\ \rho u^2 + p \\ u(E+p) \end{bmatrix},$$

with

$$E = \rho(\frac{1}{2}u^2 + e), e = e(\rho, p) = \frac{p}{(\gamma-1)\rho}, \tag{1.2}$$

where ρ is density, p is pressure, u is particle velocity , E is total energy per unit volume, e is the specific internal energy and γ is the ratio of specific heat ($\gamma = 1.4$ for ideal gas). The sound speed a is defined as

$$a = \sqrt{\frac{\gamma p}{\rho}}. \tag{1.3}$$

Physically, the density ρ and the pressure p should both be positive, and failure of preserving positive density or pressure may cause blow-up of the numerical solutions. In the past few years, many first order positivity-preserving schemes are developed, such as Godunov-type schemes [8], the flux vector splitting schemes [15], Lax-Friedrichs scheme [29,46], the HLLC scheme [2] and gas-kinetic schemes [28,38]. Some second-order schemes are developed based on these first order schemes, such as [38,29,9]. In [29], Perthame and Shu have proposed positivity-preserving first and higher order finite volume schemes for one and two dimensional compressible Euler equations. Zhang and Shu have developed positivity-preserving methods for arbitrary high-order discontinuous Galerkin (DG) methods [46,47, 49] and finite volume and finite difference WENO schemes [44,48]. In [16], Hu et. al. have developed positivity-preserving high-order conservative schemes solving compressible Euler equations. In [41], Xiong et. al have developed a parametrized positivity preserving flux limiters for finite difference RK-WENO scheme solving the compressible Euler equations.

In the present paper, a conservative positivity-preserving fifth-order finite volume compact-WENO (FVCW) scheme is proposed for compressible Euler equations. We employ the main idea that has been described in [11] where lower order compact stencils are combined with WENO weights to yield a fifth-order upwind compact interpolation. As an alternative to the finite difference compact schemes proposed in [11], we design a conservative positivity-preserving fifth-order finite volume scheme for compressible Euler equations, where the positivity-preserving scaling limiter [46,44] is used to preserve positive density and internal energy. The HLLC approximate Riemann solver [39,2] is used as the numerical flux at the element interfaces due to its robustness and accuracy for compressible Euler equations.

The rest of the paper is organized as follows. In Section 2, the positivity-preserving finite volume compact-WENO scheme for the compressible Euler equations is presented.

Numerical tests for some benchmark problems of compressible Euler equations are studied in Section 3. Conclusions are made in Section 4.

2 Positivity-preserving finite volume compact-WENO scheme

2.1 The finite volume scheme for compressible Euler equations

In this section, we first introduce the finite volume scheme [23] for compressible Euler equations (1.1) . The computational domain $[a,b]$ is divided into N cells as follows

$$a = x_{\frac{1}{2}} < x_{\frac{3}{2}} < \cdots < x_{N+\frac{1}{2}} = b.$$

The cells are denoted by $I_j = [x_{j-\frac{1}{2}}, x_{j+\frac{1}{2}}]$ and the cell size is $\Delta x_j = x_{j+\frac{1}{2}} - x_{j-\frac{1}{2}}$. If we integrate equation (1.1) over cell I_j, we obtain

$$\frac{\partial}{\partial t}\int_{x_{j-\frac{1}{2}}}^{x_{j+\frac{1}{2}}} U dx + F(U(x_{j+\frac{1}{2}},t)) - F(U(x_{j-\frac{1}{2}},t)) = 0. \tag{2.1}$$

The cell average of I_j is defined as

$$\bar{U_j} = \frac{1}{\Delta x_j}\int_{x_{j-\frac{1}{2}}}^{x_{j+\frac{1}{2}}} U(x,t)dx, \tag{2.2}$$

and the finite volume conservative scheme for (2.1) is

$$\frac{d\bar{U_j}(t)}{dt} = -\frac{1}{\Delta x_j}(\hat{F}_{j+\frac{1}{2}} - \hat{F}_{j-\frac{1}{2}}), \tag{2.3}$$

where the numerical flux $\hat{F}_{j+\frac{1}{2}}$ is a vector function of mass, momentum and total energy at the cell boundary and is defined by

$$\hat{F}_{j+\frac{1}{2}} = \hat{F}(U^-_{j+\frac{1}{2}}, U^+_{j+\frac{1}{2}}). \tag{2.4}$$

In this paper, $U^-_{j+\frac{1}{2}}$ and $U^+_{j+\frac{1}{2}}$ are obtained from a high order compact-WENO reconstruction, which will be discussed in the following subsections.

2.2 Finite volume compact-WENO scheme for scalar conservation laws

For simplicity, we consider uniform grids with cell size $\Delta x_j = h = \frac{b-a}{N}, \forall j$ in this paper. We first review the finite volume compact scheme proposed in [32]. The compact representation of $u(x)$ around the intermediate node $x_{j+\frac{1}{2}}$ can be written as

$$\sum_{l=-L_1}^{L_2} \alpha_l \tilde{u}_{j+\frac{1}{2}+l} = \sum_{m=-M_1}^{M_2} a_m \bar{u}_{j+m}, \tag{2.5}$$

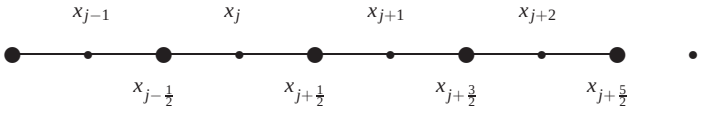

Fig. 2.1 Candidate stencils for interior points

where $\tilde{u}_{j+\frac{1}{2}}$ denotes the reconstruction value of a scalar variable $u(x)$ at the intermediate node $x_{j+\frac{1}{2}}$. Assuming that the function u can be expanded by Taylor series up to K-th order around $x_{j+\frac{1}{2}}$

$$u(x) = \sum_{n=0}^{K-1} u^{(n)}_{j+\frac{1}{2}} \frac{(x - x_{j+\frac{1}{2}})^n}{n!} + O(h^K), \tag{2.6}$$

we have

$$\tilde{u}_{j+\frac{1}{2}+l} = \sum_{n=0}^{K-1} u^{(n)}_{j+\frac{1}{2}} \frac{l^n}{n!} h^n + O(h^K), \tag{2.7}$$

$$\bar{u}_{j+m} = \sum_{n=0}^{K-1} u^{(n)}_{j+\frac{1}{2}} \frac{1}{(n+1)!} [m^{n+1} - (m-1)^{n+1}] h^n + O(h^K). \tag{2.8}$$

A fifth-order compact upwind scheme in this class is for $K = 5$, which can yield the following scheme by taking $L_1 = L_2 = M_1 = M_2 = 1$ in (2.5),

$$\frac{3}{10}\tilde{u}_{j-\frac{1}{2}} + \frac{6}{10}\tilde{u}_{j+\frac{1}{2}} + \frac{1}{10}\tilde{u}_{j+\frac{3}{2}} = \frac{1}{30}\bar{u}_{j-1} + \frac{19}{30}\bar{u}_j + \frac{10}{30}\bar{u}_{j+1}. \tag{2.9}$$

Symmetrically, we also have

$$\frac{1}{10}\tilde{u}_{j-\frac{1}{2}} + \frac{6}{10}\tilde{u}_{j+\frac{1}{2}} + \frac{3}{10}\tilde{u}_{j+\frac{3}{2}} = \frac{10}{30}\bar{u}_j + \frac{19}{30}\bar{u}_{j+1} + \frac{1}{30}\bar{u}_{j+2}. \tag{2.10}$$

These classical small length scale fifth order finite volume compact schemes (2.9) and (2.10) are very accurate and keep good resolutions in smooth regions, but unacceptable non-physical oscillations are generated when they are applied directly to some physical problems with discontinuities and the amplitude does not decrease as the grid is refined. To overcome this difficulty, a class of compact-reconstruction finite difference WENO schemes is presented in [11], where lower order compact stencils are identified at each interface and combined with WENO nonlinear weights. Comparing to the classical WENO schemes, the compact-reconstruction WENO schemes [11] have higher resolution and lower truncation errors. Across discontinuities, the schemes reduce to lower-order non-oscillatory compact schemes.

In the following, we adopt the main idea of [11] to form a finite volume compact-WENO scheme, which uses a nonlinear convex combination of all candidate stencils to reduce spurious non-physical oscillations. A fifth order finite volume compact-WENO scheme will be constructed by using three third-order compact stencils as candidates, as shown in Fig.2.1. From (2.5), for the three candidate stencils, we have

$$\begin{aligned}
\frac{2}{3}u^{(0)}_{j-\frac{1}{2}} + \frac{1}{3}u^{(0)}_{j+\frac{1}{2}} &= \frac{1}{6}(\bar{u}_{j-1} + 5\bar{u}_j), \\
\frac{1}{3}u^{(1)}_{j-\frac{1}{2}} + \frac{2}{3}u^{(1)}_{j+\frac{1}{2}} &= \frac{1}{6}(5\bar{u}_j + \bar{u}_{j+1}), \\
\frac{2}{3}u^{(2)}_{j+\frac{1}{2}} + \frac{1}{3}u^{(2)}_{j+\frac{3}{2}} &= \frac{1}{6}(\bar{u}_j + 5\bar{u}_{j+1}).
\end{aligned} \tag{2.11}$$

Given the cell averages $\{\bar{u}_j\}$, a nonlinear weighted combination of (2.11) will result in an implicit system

$$\begin{aligned}&\frac{2\omega_0+\omega_1}{3}\tilde{u}_{j-\frac{1}{2}}+\frac{\omega_0+2(\omega_1+\omega_2)}{3}\tilde{u}_{j+\frac{1}{2}}+\frac{1}{3}\omega_2\tilde{u}_{j+\frac{3}{2}}\\ =&\frac{1}{6}\omega_0\bar{u}_{j-1}+\frac{5(\omega_0+\omega_1)+\omega_2}{6}\bar{u}_j+\frac{\omega_1+5\omega_2}{6}\bar{u}_{j+1}.\end{aligned}\tag{2.12}$$

where the nonlinear weights $\{\omega_0,\omega_1,\omega_2\}$ will be specified later. Let $u^-_{j+\frac{1}{2}}$ denote the fifth order approximation of the nodal value $u(x_{j+\frac{1}{2}},t^n)$ in cell I_j. From (2.12), a fifth order compact-WENO approximation of $u^-_{j+\frac{1}{2}}$ based on the stencil $\{x_{j-1},x_j,x_{j+1}\}$ is given to be

$$u^-_{j+\frac{1}{2}}=\tilde{u}_{j+\frac{1}{2}}.\tag{2.13}$$

In smooth regions of the solution, the finite volume compact-WENO scheme yields a fifth-order upwind compact scheme [32]. In [3], a set of new smoothness indicators β^z_k is proposed as follows

$$\beta^z_k=\left(\frac{\beta_k+\varepsilon}{\beta_k+\tau_5+\varepsilon}\right),k=0,1,2,\tag{2.14}$$

where $\tau_5=|\beta_2-\beta_0|$ and the classical smooth indicators β_k $(k=0,1,2)$ [35] are given by

$$\begin{aligned}\beta_0&=\frac{13}{12}(\bar{u}_{j-2}-2\bar{u}_{j-1}+\bar{u}_j)^2+\frac{1}{4}(\bar{u}_{j-2}-4\bar{u}_{j-1}+3\bar{u}_j)^2,\\ \beta_1&=\frac{13}{12}(\bar{u}_{j-1}-2\bar{u}_j+\bar{u}_{j+1})^2+\frac{1}{4}(\bar{u}_{j-1}-\bar{u}_{j+1})^2,\\ \beta_2&=\frac{13}{12}(\bar{u}_j-2\bar{u}_{j+1}+\bar{u}_{j+2})^2+\frac{1}{4}(3\bar{u}_j-4\bar{u}_{j+1}+\bar{u}_{j+2})^2.\end{aligned}$$

The normalized nonlinear weights ω_k are chosen to be [4]

$$\omega_k=\frac{\alpha^z_k}{\sum_{l=0}^2\alpha^z_l},\quad \alpha^z_k=c_k\left(1+\left(\frac{\tau_5}{\beta_k+\varepsilon}\right)^2\right),k=0,1,2,\tag{2.15}$$

here ε is a small positive number to avoid the denominator to be 0, in our numerical tests, it is taken to be 10^{-13}. The optimal linear weights are $c_0=\frac{2}{10},c_1=\frac{5}{10},c_2=\frac{3}{10}$.

We solve the tridiagonal system (2.12) to get $u^-_{j+\frac{1}{2}}$. Following a similar procedure as above, let $u^+_{j+\frac{1}{2}}$ denote the fifth order approximation of the nodal value $u(x_{j+\frac{1}{2}},t^n)$ from cell I_{j+1}, it can be obtained by the stencil $\{x_j,x_{j+1},x_{j+2}\}$. Similar to classical WENO schemes, near critical points, the corresponding weight approaches zero and the system reduces to a biased bidiagonal system. Across the discontinuities, the fifth-order scheme yields a third-order compact scheme which has higher resolution than a third order non-compact scheme.

2.3 Finite volume compact-WENO scheme for compressible Euler equations

In this subsection, we will describe the finite volume compact-WENO scheme for compressible Euler equations. The scalar algorithm (2.12) in the previous subsection will be applied

along each characteristic field. As we know, the conservative Euler equations (1.1) can also be written in a quasi-linear form [39]

$$U_t + A(U)U_x = 0, \tag{2.16}$$

where the coefficient matrix $A(U)$ is the Jacobian matrix of $F(U)$ and can be written as

$$A(U) = \begin{bmatrix} 0 & 1 & 0 \\ -\frac{1}{2}(\gamma-3)(\frac{u_2}{u_1})^2 & (3-\gamma)(\frac{u_2}{u_1}) & \gamma-1 \\ -\frac{\gamma u_2 u_3}{u_1^2} + (\gamma-1)(\frac{u_2}{u_1})^3 & \frac{\gamma u_3}{u_1} - \frac{3}{2}(\gamma-1)(\frac{u_2}{u_1})^2 & \gamma(\frac{u_2}{u_1}) \end{bmatrix}.$$

The total specific enthalpy H is related to the specific enthalpy h, which are

$$H = \frac{E+p}{\rho} \equiv \frac{1}{2}u^2 + h, h = e + \frac{p}{\rho}. \tag{2.17}$$

The eigenvalues of the Jacobian matrix $A(U)$ are

$$\lambda_1 = u - a, \lambda_2 = u, \lambda_3 = u + a, \tag{2.18}$$

where a is the speed of sound (1.3) and the corresponding right eigenvectors are

$$r^{(1)} = \begin{bmatrix} 1 \\ u-a \\ H-ua \end{bmatrix}, r^{(2)} = \begin{bmatrix} 1 \\ u \\ \frac{1}{2}u^2 \end{bmatrix}, r^{(3)} = \begin{bmatrix} 1 \\ u+a \\ H+ua \end{bmatrix}.$$

The matrix $R(U)$ is formed by the right eigenvectors

$$R(U) = (r^{(1)}, r^{(2)}, r^{(3)}). \tag{2.19}$$

and let $L(U) = R(U)^{-1}$, then

$$L(U)A(U)R(U) = \Lambda,$$

here Λ is the diagonal matrix $\Lambda = diag(\lambda_1, \lambda_2, \lambda_3)$. Denoting $l^{(k)}$ to be the k-th row in $L(U)$, then

$$\begin{aligned} l^{(1)} &= \frac{1}{2}(c_2 + u/a, -c_1 u - 1/a, c_1), \\ l^{(2)} &= (1 - c_2, c_1 u, -c_1), \\ l^{(3)} &= \frac{1}{2}(c_2 - u/a, -c_1 u + 1/a, c_1), \end{aligned} \tag{2.20}$$

where $c_1 = (\gamma-1)/a^2$, $c_2 = \frac{1}{2}u^2 c_1$.

At the cell interface $x_{j+\frac{1}{2}}$, denote $U^-_{j+\frac{1}{2}}$ as the fifth order approximation of the nodal values at time t^n $U(x_{j+\frac{1}{2}}, t^n)$ within the cells I_j, the scalar finite volume compact-WENO reconstruction (2.12) is applied to each component of the characteristic variables $\bar{V}_j = L(U^{Roe}_{j+\frac{1}{2}})\bar{U}_j$ to obtain $U^-_{j+\frac{1}{2}}$, where $U^{Roe}_{j+\frac{1}{2}}$ denotes the Roe-average of the cell averages values $\bar{U}_j$ and $\bar{U}_{j+1}$ [39].

The present characteristic-wise finite volume compact-WENO scheme consists of the following steps:

1. At each fixed $x_{j+\frac{1}{2}}$, compute the eigenvalues (2.18) and eigenvectors (2.19) and (2.20) by using the Roe-average.

2. Compute the WENO-Z weights (2.15) by using each component of the characteristic variables $\overline{V}_j$.
3. Apply the finite volume compact-WENO scheme for the scalar equation (2.12) to the local characteristic variables

$$\begin{aligned} &a^{(k)}_{j+\frac{1}{2}} l^{(k)}_{j+\frac{1}{2}} \tilde{U}_{j-\frac{1}{2}} + b^{(k)}_{j+\frac{1}{2}} l^{(k)}_{j+\frac{1}{2}} \tilde{U}_{j+\frac{1}{2}} + c^{(k)}_{j+\frac{1}{2}} l^{(k)}_{j+\frac{1}{2}} \tilde{U}_{j+\frac{3}{2}} \\ &= d^{(k)}_{j+\frac{1}{2}} l^{(k)}_{j+\frac{1}{2}} \overline{U}_{j-1} + e^{(k)}_{j+\frac{1}{2}} l^{(k)}_{j+\frac{1}{2}} \overline{U}_j + f^{(k)}_{j+\frac{1}{2}} l^{(k)}_{j+\frac{1}{2}} \overline{U}_{j+1} \end{aligned} \tag{2.21}$$

for $k = 1,2,3$. The coefficients $a^{(k)}_{j+\frac{1}{2}}, b^{(k)}_{j+\frac{1}{2}}, c^{(k)}_{j+\frac{1}{2}}, d^{(k)}_{j+\frac{1}{2}}, e^{(k)}_{j+\frac{1}{2}}, f^{(k)}_{j+\frac{1}{2}}$ can be obtained from Step 2.
4. The equation (2.21) can be rewritten as

$$A_{j+\frac{1}{2}} \tilde{U}_{j-\frac{1}{2}} + B_{j+\frac{1}{2}} \tilde{U}_{j+\frac{1}{2}} + C_{j+\frac{1}{2}} \tilde{U}_{j+\frac{3}{2}} = D_{j+\frac{1}{2}} \overline{U}_{j-1} + E_{j+\frac{1}{2}} \overline{U}_j + F_{j+\frac{1}{2}} \overline{U}_{j+1} \tag{2.22}$$

where

$$A_{j+\frac{1}{2}} = \begin{bmatrix} a^{(1)}_{j+\frac{1}{2}} l^{(1)}_{j+\frac{1}{2}} \\ a^{(2)}_{j+\frac{1}{2}} l^{(2)}_{j+\frac{1}{2}} \\ a^{(3)}_{j+\frac{1}{2}} l^{(3)}_{j+\frac{1}{2}} \end{bmatrix}, B_{j+\frac{1}{2}} = \begin{bmatrix} b^{(1)}_{j+\frac{1}{2}} l^{(1)}_{j+\frac{1}{2}} \\ b^{(2)}_{j+\frac{1}{2}} l^{(2)}_{j+\frac{1}{2}} \\ b^{(3)}_{j+\frac{1}{2}} l^{(3)}_{j+\frac{1}{2}} \end{bmatrix}, C_{j+\frac{1}{2}} = \begin{bmatrix} c^{(1)}_{j+\frac{1}{2}} l^{(1)}_{j+\frac{1}{2}} \\ c^{(2)}_{j+\frac{1}{2}} l^{(2)}_{j+\frac{1}{2}} \\ c^{(3)}_{j+\frac{1}{2}} l^{(3)}_{j+\frac{1}{2}} \end{bmatrix}$$

$$D_{j+\frac{1}{2}} = \begin{bmatrix} d^{(1)}_{j+\frac{1}{2}} l^{(1)}_{j+\frac{1}{2}} \\ d^{(2)}_{j+\frac{1}{2}} l^{(2)}_{j+\frac{1}{2}} \\ d^{(3)}_{j+\frac{1}{2}} l^{(3)}_{j+\frac{1}{2}} \end{bmatrix}, E_{j+\frac{1}{2}} = \begin{bmatrix} e^{(1)}_{j+\frac{1}{2}} l^{(1)}_{j+\frac{1}{2}} \\ e^{(2)}_{j+\frac{1}{2}} l^{(2)}_{j+\frac{1}{2}} \\ e^{(3)}_{j+\frac{1}{2}} l^{(3)}_{j+\frac{1}{2}} \end{bmatrix}, F_{j+\frac{1}{2}} = \begin{bmatrix} f^{(1)}_{j+\frac{1}{2}} l^{(1)}_{j+\frac{1}{2}} \\ f^{(2)}_{j+\frac{1}{2}} l^{(2)}_{j+\frac{1}{2}} \\ f^{(3)}_{j+\frac{1}{2}} l^{(3)}_{j+\frac{1}{2}} \end{bmatrix}$$

Solve the 3×3 block tridiagonal system (2.22) by using the chasing method [13] to obtain $\tilde{U}_{j+\frac{1}{2}}$.

From (2.22), a fifth order compact-WENO approximation of $U^-_{j+\frac{1}{2}}$ based on the stencil $\{x_{j-1}, x_j, x_{j+1}\}$ is given to be

$$U^-_{j+\frac{1}{2}} = \tilde{U}_{j+\frac{1}{2}}. \tag{2.23}$$

Following a similar procedure as above, let $U^+_{j+\frac{1}{2}}$ denote the fifth order approximation of the nodal value $U(x_{j+\frac{1}{2}}, t^n)$ from cell I_{j+1}, it can be obtained by the stencil $\{x_j, x_{j+1}, x_{j+2}\}$.

2.4 Positivity-preserving high order schemes with HLLC approximate Riemann solver

For compressible Euler equations, the Riemann solutions consist of a contact wave and two acoustic waves, either may be a shock or a rarefaction wave. In [12], Godunov presented a first-order upwind scheme which could capture shock waves without introducing nonphysical spurious oscillations. The important part of the Godunov-type method is the exact or approximate solution of the Riemann problem. Exact solution to the Riemann problem may be difficult or too expensive to obtain, hence approximate Riemann solvers are often used to build Godunov-type numerical schemes. The HLLC Riemann solver [39, 2] has been proved to be very simple, reliable and robust. In [2], Batten et al. proposed an appropriate choice of

the acoustic wavespeeds required by HLLC and proved that the resulting numerical method resolves isolated shock and contact waves exactly and is positively conservative.

For the HLLC flux, two averaged intermediate states U_l^*, U_r^* between the two acoustic waves S_L, S_R are considered, which are separated by the contact wave, whose speed is denoted by S_M. The two-state approximate Riemann solution is defined as

$$U^{HLLC} = \begin{cases} U_l, & \text{if } S_L > 0, \\ U_l^*, & \text{if } S_L \le 0 < S_M, \\ U_r^*, & \text{if } S_M \le 0 \le S_R, \\ U_r, & \text{if } S_R < 0. \end{cases} \tag{2.24}$$

The corresponding flux is

$$F_{j+\frac{1}{2}}^{HLLC} = \begin{cases} F_l, & \text{if } S_L > 0, \\ F_l^* = F_l + S_L(U_l^* - U_l), & \text{if } S_L \le 0 < S_M, \\ F_r^* = F_r + S_r(U_r^* - U_r), & \text{if } S_M \le 0 \le S_R, \\ F_r, & \text{if } S_R < 0. \end{cases} \tag{2.25}$$

We only consider the left star state, while the right star state can be obtained symmetrically. To determine U_l^*, the following assumption has been made [2]

$$S_M = u_l^* = u_r^* = u^*. \tag{2.26}$$

which gives the contact wave velocity

$$S_M = \frac{\rho_r u_r (S_R - u_r) - \rho_l u_l (S_L - u_l) + p_l - p_r}{\rho_l (S_R - u_r) - \rho_l (S_L - u_l)}. \tag{2.27}$$

and

$$\begin{cases} \rho_l^* = \rho_l \frac{S_L - u_l}{S_L - S_M}, \\ p^* = \rho_l (u_l - S_L)(u_l - S_M) + p_l, \\ \rho_l^* u_l^* = \frac{(S_L - u_l)\rho_l u_l + (p^* - p_l)}{S_L - S_M}, \\ E_l^* = \frac{(S_L - u_l)E_l + p^* S_M}{S_L - S_M}. \end{cases} \tag{2.28}$$

To make the scheme preserving positivity, the acoustic wavespeeds are computed from

$$S_L = \min[u_l - a_l, \tilde{u}^* - \tilde{c}^*], S_R = \min[u_r + a_r, \tilde{u}^* + \tilde{c}^*], \tag{2.29}$$

where

$$\begin{cases} \tilde{u}^* = \frac{u_l + u_r R_\rho}{1 + R_\rho}, \\ \tilde{c}^* = \sqrt{(\gamma - 1)[\tilde{H}^* - \frac{1}{2}\tilde{u}^{*2}]}, \\ \tilde{H}^* = \frac{(H_l + H_r R_\rho)}{1 + R_\rho}, \\ R_\rho = \sqrt{\frac{\rho_r}{\rho_l}}. \end{cases} \tag{2.30}$$

Define the set of physically realistic states as those with positive densities and internal energies by

$$G = \left\{ U = \begin{bmatrix} \rho \\ \rho u \\ E \end{bmatrix}, \rho > 0, e = \frac{E}{\rho} - \frac{u^2}{2} > 0 \right\}, \tag{2.31}$$

then G is a convex set [2].

We consider a first order finite volume scheme

$$\bar{U}_j^{n+1} = \bar{U}_j^n - \lambda[\hat{F}(\bar{U}_j^n, \bar{U}_{j+1}^n) - \hat{F}(\bar{U}_{j-1}^n, \bar{U}_j^n)], \tag{2.32}$$

where $\hat{F}(\cdot,\cdot)$ is a HLLC flux and $\lambda = \frac{\Delta t}{h}$. For a positively conservative scheme (2.32), if $\bar{U}_j^n, j = 1,\cdots,N$ is contained in G, then $\bar{U}_j^{n+1}, j = 1,\cdots,N$ will also lie inside G. This is guaranteed by proving the intermediate states $U_l^* \in G$ if $U_l \in G$ and $U_r^* \in G$ if $U_r \in G$, because G is a convex set, for details, see [2]. In the following, the left star state will be considered, similar arguments hold for the right star state. That is, we need to prove if

$$\rho_l > 0, E_l - \frac{1}{2}\rho_l u_l^2 > 0, \tag{2.33}$$

then

$$\rho_l^* > 0, \tag{2.34}$$

and

$$E_l^* - \frac{1}{2}\rho_l^* u_l^{*2} > 0. \tag{2.35}$$

From (2.28), we can get

$$\rho_l^* = \rho_l \frac{S_L - u_l}{S_L - S_M}. \tag{2.36}$$

Since the contact velocity (2.27) is the averaged velocity, we have

$$S_L < S_M, S_L < u_l. \tag{2.37}$$

and $\rho_l^* > 0$ can be easily obtained. Using relations (2.28) and (2.37), (2.35) can be rewritten as

$$(u_l - S_L)E_l + p_l u_l - p^* S_M + \frac{((S_L - u_l) * \rho_l * u_l - p_l + p^*)^2}{2\rho_l(S_L - u_l)} > 0. \tag{2.38}$$

which is equivalent to

$$\frac{1}{2}\rho_l(S_M - u_l)^2 - p_l\frac{S_M - u_l}{u_l - S_L} + \frac{p_l}{\gamma - 1} > 0. \tag{2.39}$$

To guarantee this inequality for any value of $S_M - u_l$, the discriminant of the above quadratic function of $S_M - u_l$ should be negative, which gives the following condition

$$\frac{p_l^2}{(u_l - S_L)^2} - 2\rho_l^2 e_l < 0, \tag{2.40}$$

then

$$S_L < u_l - \frac{p_l}{\rho_l\sqrt{2e_l}} = u_l - \sqrt{\frac{\gamma-1}{2\gamma}}\sqrt{\frac{\gamma p_l}{\rho_l}} = u_l - \sqrt{\frac{\gamma-1}{2\gamma}}a_l. \tag{2.41}$$

and this is always satisfied with acoustic wavespeeds (2.29).

Remark 1 As in [46], if we consider the first order finite volume scheme (2.32) with the HLLC flux (2.25) with averaged intermediate states (2.28) solving the compressible Euler equations (1.1), this first order scheme is positivity-preserving with the choice of the acoustic wavespeeds (2.29) under the following CFL condition

$$\lambda \, \| |u| + a \|_\infty \leq 1. \tag{2.42}$$

Now to design a positivity-preserving fifth-order finite volume compact-WENO scheme, we first consider the Euler forward time discretization for equations (2.3)

$$\bar{U}_j^{n+1} = \bar{U}_j^n - \lambda(\hat{F}(U^-_{j+\frac{1}{2}}, U^+_{j+\frac{1}{2}}) - \hat{F}(U^-_{j-\frac{1}{2}}, U^+_{j-\frac{1}{2}}) \tag{2.43}$$

where $\hat{F}$ is the HLLC flux, $U^-_{j+\frac{1}{2}}$ and $U^+_{j+\frac{1}{2}}$ are obtained by using the compact-WENO schemes in Section 2.3. We employ the idea in [44,46] to construct high order finite volume compact-WENO schemes to preserve positive density and pressure or internal energy for the Euler system.

As in [46], we consider a polynomial vector $Q_j(x) = (\rho_j(x)), (\rho u)_j(x), E_j(x))^T$ with degree $K(K \geq 2)$ on I_j, such that

$$U^+_{j-\frac{1}{2}} = Q_j(x_{j-\frac{1}{2}}), U^-_{j+\frac{1}{2}} = Q_j(x_{j+\frac{1}{2}}), \bar{U}_{j+q} = \frac{1}{\Delta x}\int_{x_{j+q-\frac{1}{2}}}^{x_{j+q+\frac{1}{2}}} Q_j(x)dx, \tag{2.44}$$

here q depends on degree K, for example, if $K = 3$, $q = 0$ and if $K = 5$, $q = -1, 0, 1$. By using the M-point Gauss-Lobatto quadrature rule on I_j and choose the quadrature points as $S_j = \{x_{j-\frac{1}{2}} = \hat{x}_j^1, \cdots, \hat{x}_j^M = x_{j+\frac{1}{2}}\}$, a sufficient condition for $\bar{U}_j^{n+1} \in G$ is $Q_j(\hat{x}_j^\alpha) \in G$ for $\alpha = 1, 2, \cdots, M$, under a suitable CFL condition. We denote $\hat{\omega}_\alpha$ as the Legendre Gauss-Lobatto quadrature weights on the interval $[-\frac{1}{2}, \frac{1}{2}]$, and $\sum_{\alpha=1}^M \hat{\omega}_\alpha = 1$ with $2M - 3 \leq K$. Following [46], we have

Theorem 1 *Consider the high order ($K \geq 2$) finite volume compact-WENO scheme (2.43) with the HLLC flux (2.25) for solving the compressible Euler equations (1.1). The first order scheme (2.32) with the HLLC flux would be positivity-preserving under the condition (2.29) with the averaged intermediate states (2.28). If the reconstructed polynomial vector $Q_j(x) = (\rho_j(x)), (\rho u)_j(x), E_j(x)$ (2.44) satisfies $Q_j(\hat{x}_j^\alpha) \in G$, the scheme (2.43) is positivity-preserving ($\bar{U}_j^{n+1} \in G$) under the the CFL condition*

$$\lambda \, \| |u| + a \|_\infty \leq \omega_1. \tag{2.45}$$

Proof The proof is similar to that in [46]. By using the M-point Gauss-Lobatto rule, the cell average $\bar{U}_j$ can be written as

$$\bar{U}_j = \frac{1}{\Delta x}\int_{x_{j-\frac{1}{2}}}^{x_{j+\frac{1}{2}}} Q_j(x)dx = \sum_{\alpha=1}^M \hat{\omega}_\alpha Q_j(\hat{x}_j^\alpha). \tag{2.46}$$

The scheme (2.43) can be rearranged as follows

$$\begin{aligned}
\bar{U}_j^{n+1} &= \sum_{\alpha=1}^M \hat{\omega}_\alpha Q_j(\hat{x}_j^\alpha) - \lambda(\hat{F}(U^-_{j+\frac{1}{2}}, U^+_{j+\frac{1}{2}}) - \hat{F}(U^+_{j-\frac{1}{2}}, U^-_{j+\frac{1}{2}}) + \hat{F}(U^+_{j-\frac{1}{2}}, U^-_{j+\frac{1}{2}}) - \hat{F}(U^-_{j-\frac{1}{2}}, U^+_{j-\frac{1}{2}})) \\
&= \sum_{\alpha=2}^{M-1} \hat{\omega}_\alpha Q_j(\hat{x}_j^\alpha) + \hat{\omega}_1 \left(U^+_{j-\frac{1}{2}} - \frac{\lambda}{\hat{\omega}_1}[\hat{F}(U^+_{j-\frac{1}{2}}, U^-_{j+\frac{1}{2}}) - \hat{F}(U^-_{j-\frac{1}{2}}, U^+_{j-\frac{1}{2}})] \right) \\
&\quad + \hat{\omega}_M \left(U^-_{j+\frac{1}{2}} - \frac{\lambda}{\hat{\omega}_M}[\hat{F}(U^-_{j+\frac{1}{2}}, U^+_{j+\frac{1}{2}}) - \hat{F}(U^+_{j-\frac{1}{2}}, U^-_{j+\frac{1}{2}})] \right) \\
&= \sum_{\alpha=2}^{M-1} \hat{\omega}_\alpha Q_j(\hat{x}_j^\alpha) + \hat{\omega}_1 H_1 + \hat{\omega}_M H_M,
\end{aligned}$$

where

$$H_1 = U^+_{j-\frac{1}{2}} - \frac{\lambda}{\hat{\omega}_1}[\hat{F}(U^+_{j-\frac{1}{2}}, U^-_{j+\frac{1}{2}}) - \hat{F}(U^-_{j-\frac{1}{2}}, U^+_{j-\frac{1}{2}})],$$
$$H_M = U^-_{j+\frac{1}{2}} - \frac{\lambda}{\hat{\omega}_M}[\hat{F}(U^-_{j+\frac{1}{2}}, U^+_{j+\frac{1}{2}}) - \hat{F}(U^+_{j-\frac{1}{2}}, U^-_{j+\frac{1}{2}})].$$

Notice that the above two equations are both of the form (2.32), therefore H_1 and H_M are in the set G under the CFL condition (2.45) with the HLLC flux (2.25) and the acoustic wavespeeds (2.29).

Motivated by the approach in [46,29], the positivity-preserving limiter for the present scheme in the one-dimensional space will be constructed. The easy implementation algorithm of WENO schemes in [44] will be adopted.

1. Set up a small positive parameter $\varepsilon = \min_j\{10^{-15}, \bar{\rho}^n_j\}$.
2. Compute the limiter
$$\theta_1 = \min\left\{\frac{\bar{\rho}^n_j - \varepsilon}{\bar{\rho}^n_j - \rho_{min}}, 1\right\}, \tag{2.47}$$
where $\rho_{min} = \{\rho^-_{j+\frac{1}{2}}, \rho^+_{j-\frac{1}{2}}, \rho_j(x^{1*}_j)\}$ and
$$\rho_j(x^{1*}_j) = \frac{\bar{\rho}^n_j - \hat{\omega}_1\rho^+_{j-\frac{1}{2}} - \hat{\omega}_M\rho^-_{j+\frac{1}{2}}}{1-2\hat{\omega}_1}. \tag{2.48}$$
3. Modify the density by using the limiter θ_1, let
$$\hat{\rho}_j(x) = \theta_1(\rho_j(x) - \bar{\rho}^n_j) + \bar{\rho}^n_j. \tag{2.49}$$
Get $\hat{\rho}^-_{j+\frac{1}{2}}$ and $\hat{\rho}^+_{j-\frac{1}{2}}$ by
$$\hat{\rho}^-_{j+\frac{1}{2}} = \theta_1(\rho^-_{j+\frac{1}{2}} - \bar{\rho}^n_j) + \bar{\rho}^n_j,$$
$$\hat{\rho}^+_{j-\frac{1}{2}} = \theta_1(\rho^+_{j-\frac{1}{2}} - \bar{\rho}^n_j) + \bar{\rho}^n_j.$$
Denote
$$\hat{W}^1_j = \hat{U}^-_{j+\frac{1}{2}} = (\hat{\rho}^-_{j+\frac{1}{2}}, (\rho u)^-_{j+\frac{1}{2}}, E^-_{j+\frac{1}{2}})^T,$$
$$\hat{W}^2_j = \hat{U}^+_{j-\frac{1}{2}} = (\hat{\rho}^+_{j-\frac{1}{2}}, (\rho u)^+_{j-\frac{1}{2}}, E^+_{j-\frac{1}{2}})^T,$$
$$\hat{W}^3_j = (\hat{\rho}_j(x^{1*}_j), (\rho u)_j(x^{2*}_j), E_j(x^{3*}_j))^T = \frac{\bar{U}^n_j - \hat{\omega}_1\hat{U}^+_{j-\frac{1}{2}} - \hat{\omega}_M\hat{U}^-_{j+\frac{1}{2}}}{1-2\hat{\omega}_1}.$$
4. Get $\theta_2 = \min_{\alpha=1,2,3} t^\alpha_\varepsilon$ by modifying the internal energy as follows:
For $\alpha = 1,2,3$:
   - if $e(\hat{W}^\alpha_j) < \varepsilon$, solve the following quadratic equations for t^α_ε as in [46]
   $$e[(1-t^\alpha_\varepsilon)\bar{U}^n_j + t^\alpha_\varepsilon\hat{W}^\alpha_j] = \varepsilon \tag{2.50}$$
   - If $e(\hat{W}^\alpha_j) \geq \varepsilon$, let $t^\alpha_\varepsilon = 1$.

Denote

$$\tilde{U}^-_{j+\frac{1}{2}} = \theta_2(\hat{U}^-_{j+\frac{1}{2}} - \bar{U}^n_j) + \bar{U}^n_j,$$
$$\tilde{U}^+_{j-\frac{1}{2}} = \theta_2(\hat{U}^+_{j-\frac{1}{2}} - \bar{U}^n_j) + \bar{U}^n_j.$$

5. The scheme (2.43) with the positivity-preserving limiter would be

$$\bar{U}^{n+1}_j = \bar{U}^n_j - \lambda(\hat{F}(\tilde{U}^-_{j+\frac{1}{2}}, \tilde{U}^+_{j+\frac{1}{2}}) - \hat{F}(\tilde{U}^-_{j-\frac{1}{2}}, \tilde{U}^+_{j-\frac{1}{2}}). \tag{2.51}$$

Remark 2 To prove that the limiter will not destroy the high order accuracy of density for smooth solutions, for a fifth order scheme, we need to show $\hat{\rho}_j(x) - \rho_j(x) = O(\Delta x^5)$ in (2.49). In the present compact scheme, although $\rho^-_{j+\frac{1}{2}}$ and $\rho^+_{j-\frac{1}{2}}$ are obtained globally, which are different from those in [45,46], the constructed polynomial $\rho_j(x)$ from (2.44) can be seen locally. Thus, the proof of preserving high order accuracy of density is similar to that in [45, 46]. Similar arguments hold for the internal energy. So the scheme (2.51) is conservative, high order accurate and positivity preserving.

2.5 Temporal discretization

Strong stability preserving (SSP) high order Runge-Kutta time discretization [14] will be used to improve the temporal accuracy for the scheme (2.51). The third-order SSP Runge-Kutta method is

$$\begin{aligned} U^{(1)} &= U^n + \Delta t L(U^n) \\ U^{(2)} &= \frac{3}{4}U^n + \frac{1}{4}U^{(1)} + \frac{1}{4}\Delta t L(U^{(1)}) \\ U^{n+1} &= \frac{1}{3}U^n + \frac{2}{3}U^{(2)} + \frac{2}{3}\Delta t L(U^{(2)}), \end{aligned} \tag{2.52}$$

where $L(U)$ is the spatial operator. Similar to [46], for SSP high order time discretizations, the limiter will be used at each stage on each time step.

3 Numerical examples

In this section, we will investigate the numerical performance of the present positivity-preserving fifth-order finite volume compact-WENO (FVCW) scheme. The fifth-order WENO scheme [4] will be denoted as "WENO-Z" and the original fifth order WENO scheme of Jiang and Shu [17] is denoted as "WENO-JS". We will compare the FVCW scheme to WENO-JS and WENO-Z schemes. For all the numerical tests, the third-order SSP Runge-Kutta method (2.52) is used under the CFL condition (2.45).

Example 1 Advection of density perturbation. The initial conditions for density, velocity and pressure are specified, respectively, as

$$\rho(x,0) = 1 + 0.2sin(\pi x), u(x,0) = 1, p(x,0) = 1.$$

The exact solution of density is $\rho(x,t) = 1 + 0.2sin(\pi(x-t))$.

The computational domain is $[0,2]$ and the boundary condition is periodic. The L_1, L_2 and L_∞ errors and orders at $t = 2$ for the present finite volume compact-WENO scheme are shown in Table 1. We clearly observe fifth-order accuracy for this problem.

Table 3.1 Numerical errors and orders for Example 1.

N	L_1 error	L_1 Order	L_∞ error	L_∞ Order	L_2 error	L_2 Order
10	7.802E-04		6.506E-04		5.874E-04	
20	1.493E-05	5.71	1.716E-05	5.24	1.263E-05	5.54
40	3.260E-07	5.52	2.942E-07	5.87	2.625E-07	5.59
80	9.107E-09	5.16	9.117E-09	5.01	7.162E-09	5.20
160	2.695E-10	5.08	2.903E-10	4.97	2.113E-10	5.08
320	8.169E-12	5.04	9.202E-12	4.98	6.413E-12	5.04

Example 2 This example is the one-dimensional shock tube test of Lax [21] with the following Riemann initial condition

$$(\rho,u,p)=\begin{cases}(0.445,0.698,3.528), & -5\le x<0,\\ (0.5,0,0.571), & 0\le x<5,\end{cases} \tag{3.1}$$

and the final time is $t=1.4$.

The Lax problem is a difficult shock tube problem. The exact solutions contain shock, contact discontinuity and rarefaction wave. We compute the solution on the domain $[-5,5]$ with Neumann boundary conditions. The density and pressure on a grid of 200 points for the WENO-JS, WENO-Z and the present finite volume compact schemes are shown in Fig. 3.1. For this test problem, we observe that FVCW scheme is sharper than the WENO-JS and WENO-Z schemes, as it is less dissipative.

Example 3 This example is the one-dimensional shock tube test of Sod [37] with the following Riemann initial condition

$$(\rho,u,p)=\begin{cases}(0.125,0,1), & -5\le x<0,\\ (1,0,1), & 0\le x<5,\end{cases} \tag{3.2}$$

and the final time is $t=2.0$.

The exact solution contains a left-running rarefaction wave and right-running contact discontinuity and shock wave. The spatial domain $[-5,5]$ is discretized with 100 grid points and the results are shown in Fig.3.2. We compare our numerical results with those obtained by WENO-JS and WENO-Z schemes. The present scheme can capture the shock front and contact discontinuity with correct locations and satisfactory sharpness. From Fig.3.2(b,c), we can observe that the numerical results obtained by the present FVCW scheme shows significant lower smearing across the discontinuity.

Example 4 In this example, the one dimensional Mach 3 shock-turbulence wave interaction [36] is tested with the following initial conditions

$$(\rho,u,p)=\begin{cases}(3.857143,2.629369,10.33333), & -5\le x<-4,\\ (1+0.2\sin 5x,0,1), & -4\le x<5,\end{cases} \tag{3.3}$$

and the final time is $t=1.8$. The solution of this problem consists of the interaction of a stationary shock and fine scale structures which are located behind a right-going main shock. As the density perturbation passes through the shock, it produces perturbations developing into shocks with smaller amplitude. Fig.3.3 shows the density on a grid of 200 points for the WENO-JS, WENO-Z and FVCW schemes. The "exact solution" is a reference solution computed by the WENO-JS scheme with 3200 grid points. It is observed that the present finite volume compact scheme captures the fine scale structures of the solution

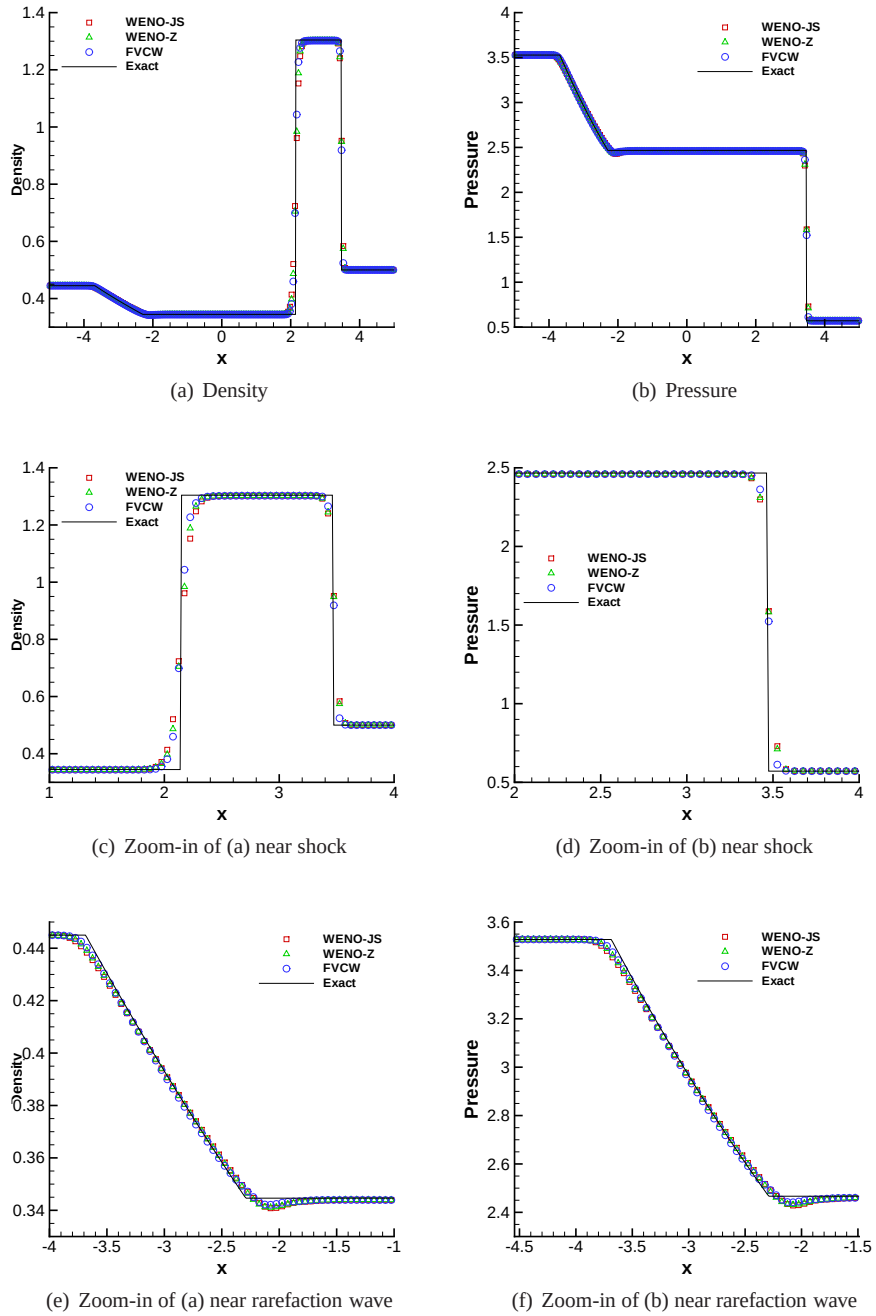

(a) Density (b) Pressure

(c) Zoom-in of (a) near shock (d) Zoom-in of (b) near shock

(e) Zoom-in of (a) near rarefaction wave (f) Zoom-in of (b) near rarefaction wave

Fig. 3.1 The density (left) and pressure (right) profiles of the Lax problem (3.1) at $t = 1.4$.

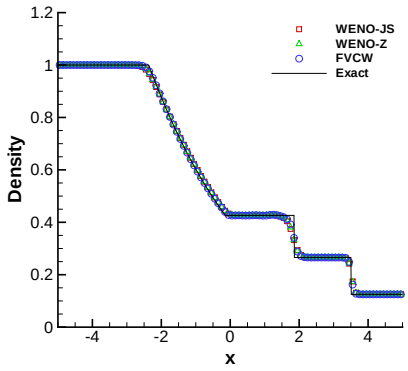

(a) Density

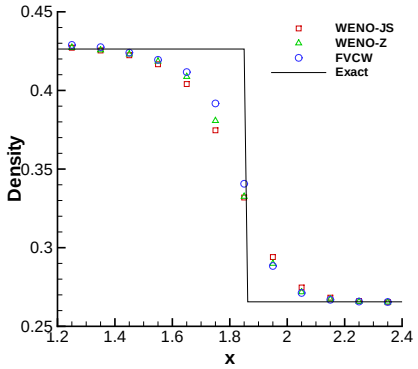

(b) Zoom-in of (a) near shock

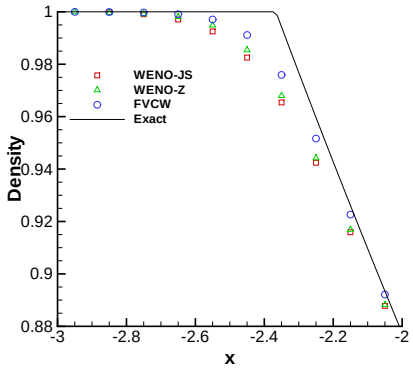

(c) Zoom-in of (a) near rarefaction wave

Fig. 3.2 The density profiles of the Sod problem (3.2) at $t = 2.0$.

at the high-frequency waves behind the shock better than WENO-JS and WENO-Z, while also maintaining non-oscillatory behavior across the shock wave. The numerical solution is greatly improved with $N = 400$ and the numerical results are shown in Fig. 3.4.

Example 5 The one dimensional blastwave interaction problem of Woodward and Collela [40] has the following initial condition

$$(\rho, u, p) = \begin{cases} (1, 0, 1000), & 0 \le x < 0.1, \\ (1, 0, 0.01), & 0.1 \le x < 0.9, \\ (1, 0, 100), & 0.9 \le x \le 1.0, \end{cases} \tag{3.4}$$

and boundary conditions are reflective. The final time is $t = 0.038$. The initial pressure gradients generate two density shock waves that collide and interact at later time. The solution of this problem contains rarefactions, interaction of shock waves and the collision of strong shock waves. The "exact solution" of this test problem is a reference solution computed by the WENO-JS scheme with 3200 grid. The density obtained with WENO-JS, WENO-Z and

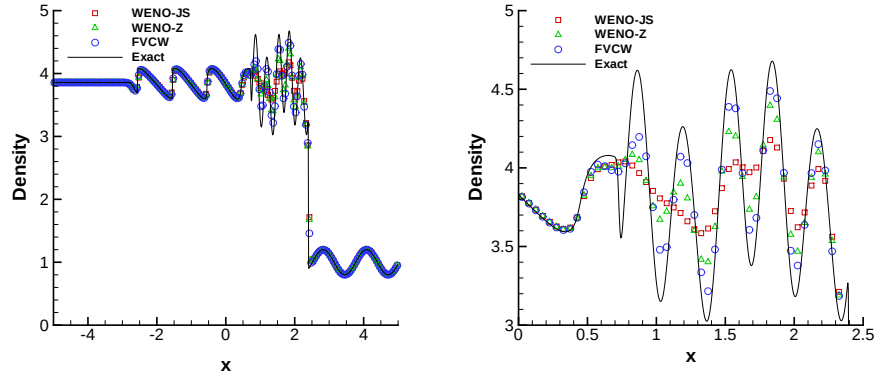

(a) Density: $N = 200$ (b) Zoom-in of (a) near shock-turbulence wave

Fig. 3.3 Shock-turbulence interaction (3.3) with $N = 200$ at $t = 1.8$.

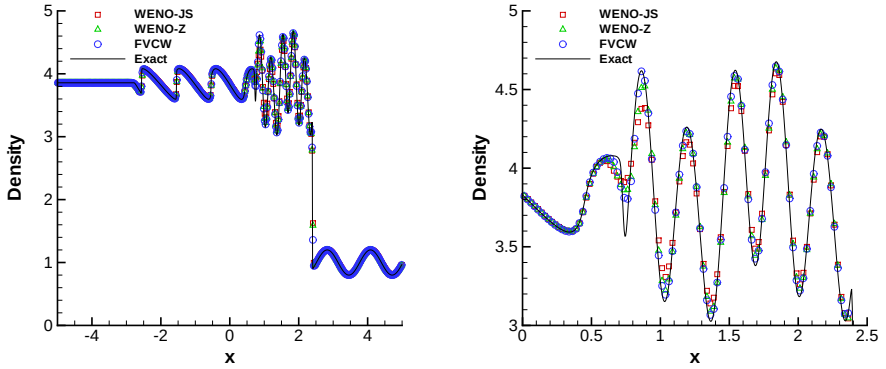

(a) Density: $N = 400$ (b) Zoom-in of (a) near shock-turbulence wave.

Fig. 3.4 Shock-turbulence interaction (3.3) with $N = 400$ at $t = 1.8$.

the present FVCW schemes at $t = 0.038$ with 200 cells are shown in Fig. 3.5. The zoomed regions of the density profile Fig. 3.5 (b) show that the present FVCW scheme gives better resolution than the other two schemes. The numerical solution is also greatly improved with $N = 400$ and the numerical results are shown in Fig. 3.6.

Example 6 In this test, we consider one-dimensional low density and low internal energy Riemann problem with the following initial condition

$$(\rho, u, p) = \begin{cases} (1, -2, 0.4), & 0 \le x < 0.5, \\ (1, 2, 0.4), & 0.5 \le x < 1, \end{cases} \tag{3.5}$$

with $h = 0.0025$ and the final time is $t = 0.1$. The exact solution of this test consists of a trivial contact wave and two symmetric rarefaction waves. The results of the present positivity-preserving FVCW scheme with 400 cells compared with the exact solution are shown in Fig. 3.7. The minimum numerical values of the density and the internal energy are $1.835E-02$

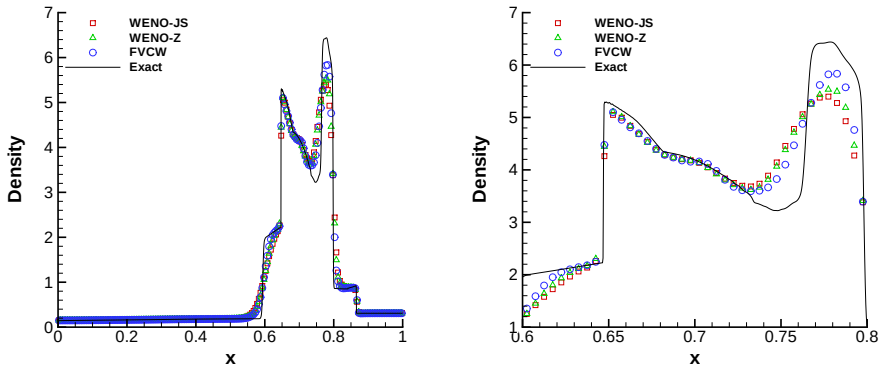

(a) Density: $N = 200$ (b) Zoom-in of (a) at the complex smooth region.

Fig. 3.5 Blastwave interaction problem (3.4) with $N = 200$ at $t = 0.038$.

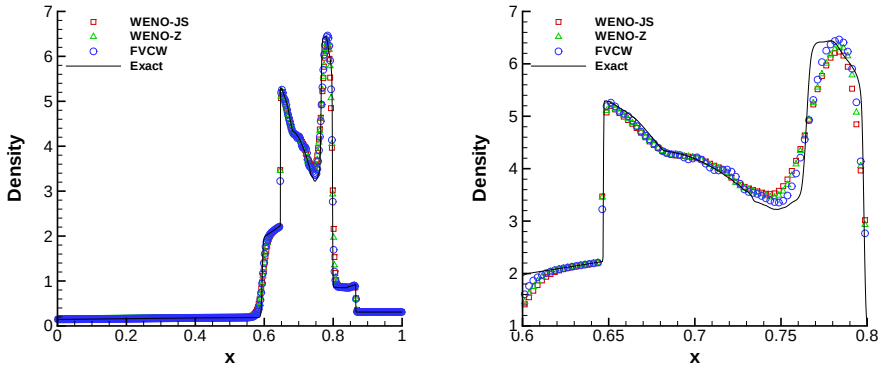

(a) Density: $N = 400$ (b) Zoom-in of (a) at the complex smooth region.

Fig. 3.6 Blastwave interaction problem (3.4) with $N = 400$ at $t = 0.038$.

and $3.158E-01$ respectively. The numerical solutions for this low density and low internal energy problem can capture the exact solutions comparably well.

Example 7 In this test, a strong shock wave is generated by an extremely high pressure in the initial condition

$$(\rho,u,p) = \begin{cases} (1,0,10^{10}), & 0 \le x \le 0.5, \\ (0.125,0,0.1), & 0.5 \le x < 1. \end{cases} \tag{3.6}$$

with the final time is $t = 2.5 \times 10^{-6}$. The results of the present positivity-preserving FVCW scheme with 200 cells compared with the exact solution are shown in Fig.3.8. The numerical solutions are very satisfactory in regard to numerical diffusion and spurious oscillations. The minimum numerical values of the density and the internal energy for this problem are $1.250E-01$ and $2.000E+00$ respectively. Both are positive.

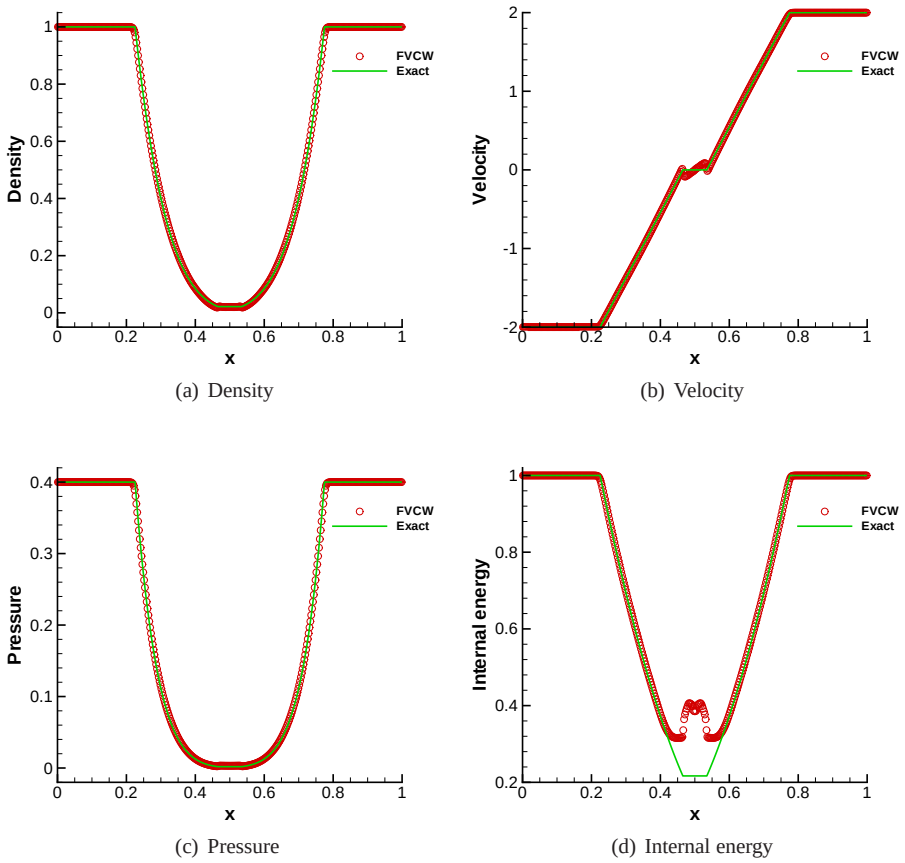

(a) Density (b) Velocity

(c) Pressure (d) Internal energy

Fig. 3.7 The results of the low density and low internal energy problem (3.5) with $N = 400$ at $t = 0.1$.

Example 8 This one-dimensional test problem involves vacuum or near-vacuum solutions with the following initial condition

$$(\rho, u, p) = \begin{cases} (7, -1, 0.2), & -1 \le x < 0, \\ (7, -1, 0.2), & 0 \le x \le 1, \end{cases} \tag{3.7}$$

with $h = 0.005$ and the final time is $t = 0.6$. The computed pressure, density and velocity distributions are show in Fig. 3.9 (left). For this double rarefaction problem, the present FVCW scheme with the HLLC flux has comparable results as those in Zhang and Shu [48] (see their Fig. 5.1 (left)). The minimum numerical values of the density and the internal energy are small positive values of $2.120E-04$ and $2.201E-04$ respectively.

Example 9 This one-dimensional test problem is the planar Sedov blast-wave problem with the following initial condition

$$(\rho, u, p) = \begin{cases} (1, 0, 4 \times 10^{-13}), & 0 < x \le 2 - 0.5h, \ 2 + 0.5h < x < 4, \\ (1, 0, 2.56 \times 10^{8}), & 2 - 0.5h < x \le 2 + 0.5h, \end{cases} \tag{3.8}$$

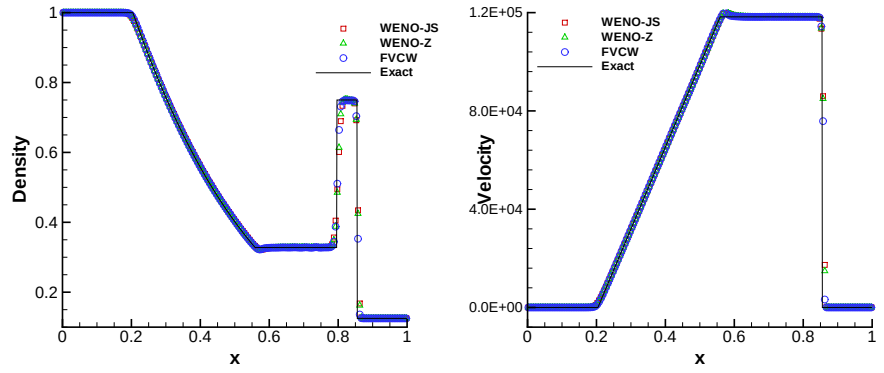

(a) Density

(b) Velocity

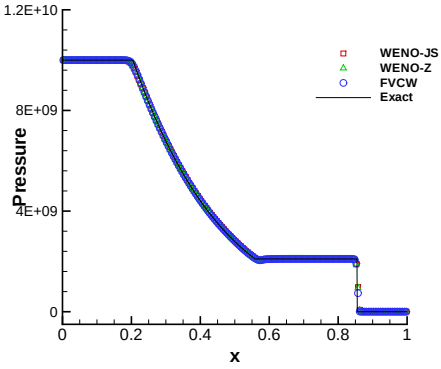

(c) Pressure

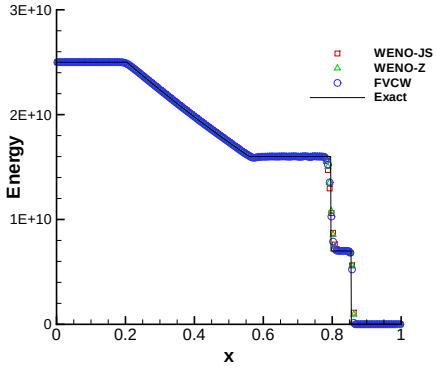

(d) Internal energy

Fig. 3.8 The results of the strong shock wave problem (3.6) with $N = 200$ at $t = 2.5 \times 10^{-6}$.

with $h = 0.005$ and the final time is $t = 0.001$. The numerical results of the present positivity-preserving fifth order finite volume compact-WENO scheme are shown in Fig.3.9 (right). By comparing with Zhang and Shu [48] (see their Fig. 5.1 (right)) for the planar Sedov blast-wave problem, we can observe that a slightly sharper blast wave is obtained by using the present FVCW scheme. The minimum numerical values of the density and the internal energy are also small positive values of $4.731E-03$ and $1.000E-12$ respectively.

Example 10 LeBlanc shock tube problem. In this extreme shock tube problem, the computational domain is [0,9] filled with a perfect gas with $\gamma = 5/3$. The initial conditions are with high ratio of jumps for the internal energy and density. The jump for pressure is 10^9 and the jump for density is 10^3. The initial conditions are given by

$$(\rho, u, e) = \begin{cases} (1, 0, 0.1), & 0 \le x < 3, \\ (0.001, 0, 10^{-7}), & 3 < x \le 9. \end{cases} \tag{3.9}$$

The solution consists of a strong rarefaction wave moving to the left, a contact discontinuity and a shock moving to the right. The discussion of the difficulties in the numerical

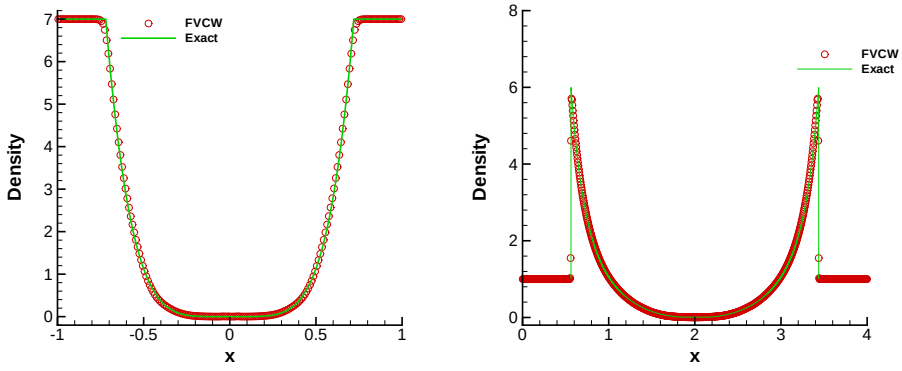

(a) Density

(b) Density

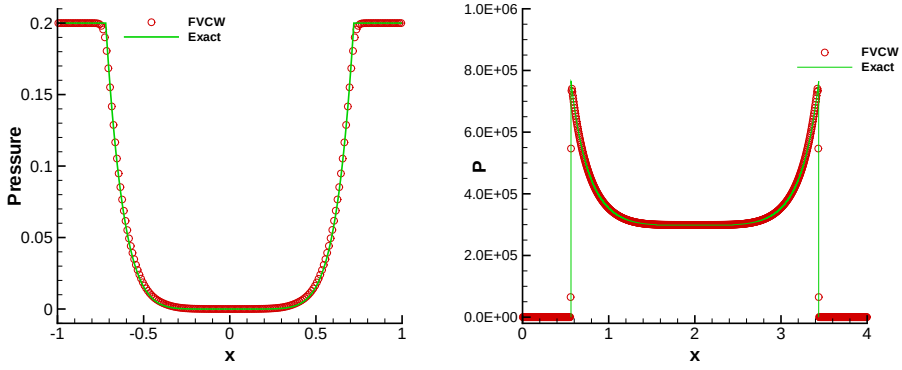

(c) Pressure

(d) Pressure

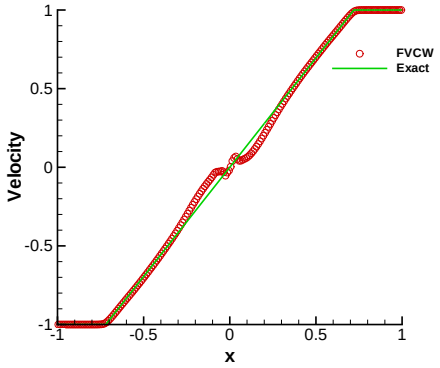

(e) Velocity

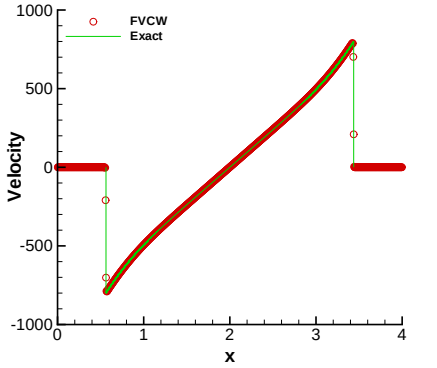

(f) Velocity

Fig. 3.9 One-dimensional problems involving vacuum or near vacuum, $h = 0.005$: (left) double rarefaction problem (3.7) at $t = 0.6$; (right) planar Sedov blast-wave problem (3.8) at $t = 0.001$.

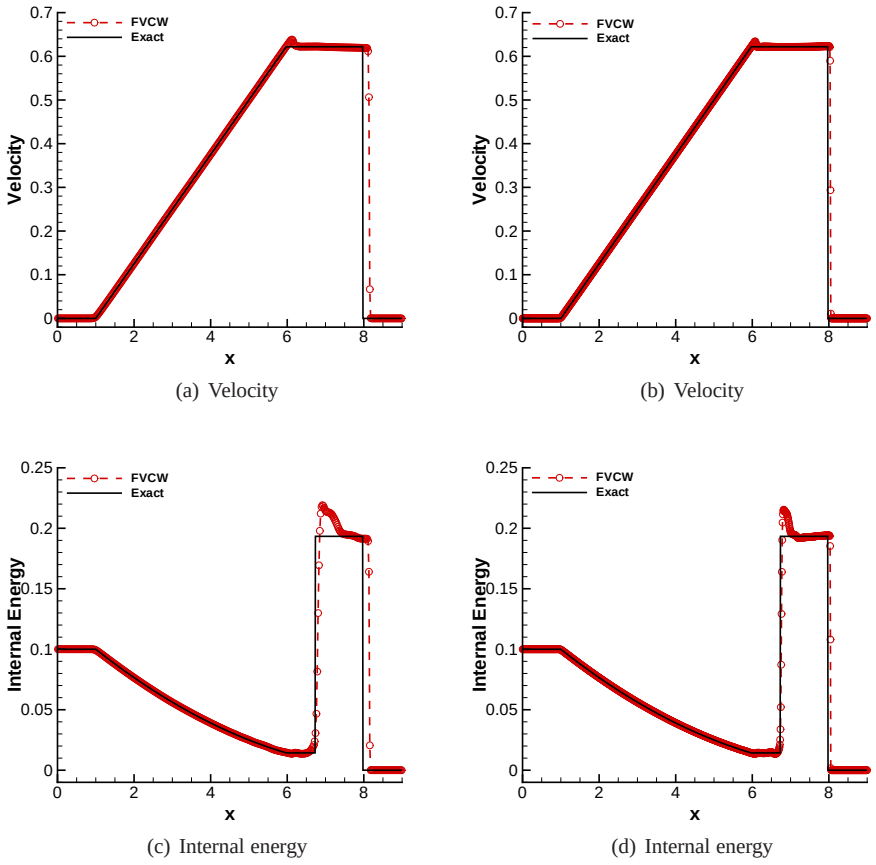

(a) Velocity (b) Velocity

(c) Internal energy (d) Internal energy

Fig. 3.10 The results of the Leblanc problem (3.9) at $t = 6.0$. $N = 400$ (left), $N = 1000$ (right).

simulation of this problem can be found in [24, 5, 27]. Numerical results obtained with the present FVCW schemes at $t = 6.0$ with 400 and 1000 cells are shown in Fig.3.10. By comparing with the exact solutions, we can observe that the present FVCW scheme preserves positive density and internal energy, and the minimum numerical values for density and pressure are $1.000E-03$ and $1.000E-07$ respectively. A slight overshoot is produced, especially for the internal energy, however similar results are obtained in [24, 5, 27]. Fig.3.10 shows that the numerical solution is greatly improved as the mesh is refined.

4 Conclusions

In this paper, we develop a positivity-preserving fifth-order finite volume compact-WENO scheme for compressible Euler equations of fluid dynamics in one dimension based on the idea of finite volume WENO schemes and classical compact schemes. Compared to finite difference compact-reconstruction WENO schemes proposed by Ghosh et. al. [11], the positivity-preserving limiter is used to preserve positive density and internal energy un-

der a finite volume framework. An approximate HLLC Riemann solver is used due to its efficiency, robustness and accuracy. The present scheme increases the accuracy and spectral properties of the classical WENO schemes for a given order of convergence. Compared to classical small length scale fifth order finite volume compact schemes, the present scheme keeps the essentially non-oscillatory properties for capturing discontinuities. Numerical results have shown that the present scheme is positivity preserving, high order accurate, and can produce superior resolutions and lower truncation errors compared to the classical WENO schemes. Extension the FVCW scheme to multi-dimensional problems contributes our future work.

Acknowledgements The work was partly supported by the Fundamental Research Funds for the Central Universities (2010QNA39, 2010LKSX02). The third author acknowledges the funding support of this research by the Fundamental Research Funds for the Central Universities(2012QNB07).

References

1. Adams, N., Shariff, K.: A high-resolution hybrid compact-ENO scheme for shock-turbulence interaction problems. Journal of Computational Physics **127**(1), 27–51 (1996)
2. Batten, P., Clarke, N., Lambert, C., Causon, D.: On the choice of wavespeeds for the HLLC Riemann solver. SIAM Journal on Scientific Computing **18**(6), 1553–1570 (1997)
3. Borges, R., Carmona, M., Costa, B., Don, W.: An improved weighted essentially non-oscillatory scheme for hyperbolic conservation laws. Journal of Computational Physics **227**(6), 3191–3211 (2008)
4. Castro, M., Costa, B., Don, W.: High order weighted essentially non-oscillatory WENO-Z schemes for hyperbolic conservation laws. Journal of Computational Physics **230**(5), 1766–1792 (2011)
5. Cheng, J., Shu, C.W.: Positivity-preserving Lagrangian scheme for multi-material compressible flow. Journal of Computational Physics **257**(0), 143–168 (2014)
6. Deng, X., Maekawa, H.: Compact high-order accurate nonlinear schemes. Journal of Computational Physics **130**(1), 77–91 (1997)
7. Deng, X., Zhang, H.: Developing high-order weighted compact nonlinear schemes. Journal of Computational Physics **165**(1), 22–44 (2000)
8. Einfeldt, B., Munz, C.D., Roe, P.L., Sjögreen, B.: On Godunov-type methods near low densities. Journal of Computational Physics **92**(2), 273–295 (1991)
9. Estivalezes, J., Villedieu, P.: High-order positivity-preserving kinetic schemes for the compressible euler equations. SIAM Journal on Numerical Analysis **33**(5), 2050–2067 (1996)
10. Gaitonde, D., Shang, J.: Optimized compact-difference-based finite-volume schemes for linear wave phenomena. Journal of Computational Physics **138**(2), 617–643 (1997)
11. Ghosh, D., Baeder, J.: Compact Reconstruction Schemes with Weighted ENO Limiting for Hyperbolic Conservation Laws. SIAM Journal on Scientific Computing **34**(3), 1678–1706 (2012)
12. Godunov, S.K.: A differerence method for the numerical calculation of discontinuous solutions of hydrodynamic equations. Mathematicheskii Sbornik **89**(3), 271–306 (1959)
13. Gong, Y., Long, Y.X.: LU method for solving block tridiagonal matrix equations and its applications. Journal of Dalian University of Technology **37**(4), 406–409 (1997)
14. Gottlieb, S., Ketcheson, D., Shu, C.W.: High order strong stability preserving time discretizations. Journal of Scientific Computing **38**(3), 251–289 (2009)
15. Gressier, J., Villedieu, P., Moschetta, J.M.: Positivity of flux vector splitting schemes. Journal of Computational Physics **155**(1), 199–220 (1999)
16. Hu, X.Y., Adams, N.A., Shu, C.W.: Positivity-preserving method for high-order conservative schemes solving compressible euler equations. Journal of Computational Physics (2013)
17. Jiang, G.S., Shu, C.W.: Efficient implementation of weighted ENO schemes. Journal of Computational Physics **126**(1), 202–228 (1996)
18. Jiang, L., Shan, H., Liu, C.: Weighted compact scheme for shock capturing. International Journal of Computational Fluid Dynamics **15**(2), 147–155 (2001)
19. Kobayashi, M.: On a class of Padé finite volume methods. Journal of Computational Physics **156**(1), 137–180 (1999)
20. Lacor, C., Smirnov, S., Baelmans, M.: A finite volume formulation of compact central schemes on arbitrary structured grids. Journal of Computational Physics **198**(2), 535–566 (2004)

21. Lax, P.D.: Weak solutions of nonlinear hyperbolic equations and their numerical computation. Communications on Pure and Applied Mathematics **7**(1), 159–193 (1954)
22. Lele, S.: Compact finite difference schemes with spectral-like resolution. Journal of Computational Physics **103**(1), 16–42 (1992)
23. LeVeque, R.: Finite volume methods for hyperbolic problems. Meccanica **39**, 88–89 (2004)
24. Liu, W., Cheng, J., Shu, C.W.: High order conservative Lagrangian schemes with Lax–Wendroff type time discretization for the compressible Euler equations. Journal of Computational Physics **228**(23), 8872–8891 (2009)
25. Liu, X., Osher, S., Chan, T.: Weighted essentially non-oscillatory schemes. Journal of Computational Physics **115**(1), 200–212 (1994)
26. Liu, X., Zhang, S., Zhang, H., Shu, C.W.: A new class of central compact schemes with spectral-like resolution i: Linear schemes. Journal of Computational Physics **248**, 235256 (2013)
27. Loubère, R., Shashkov, M.J.: A subcell remapping method on staggered polygonal grids for arbitrary-Lagrangian–Eulerian methods. Journal of Computational Physics **209**(1), 105–138 (2005)
28. Perthame, B.: Boltzmann type schemes for gas dynamics and the entropy property. SIAM Journal on Numerical Analysis **27**(6), 1405–1421 (1990)
29. Perthame, B., Shu, C.W.: On positivity preserving finite volume schemes for Euler equations. Numerische Mathematik **73**(1), 119–130 (1996)
30. Piller, M., Stalio, E.: Finite-volume compact schemes on staggered grids. Journal of Computational Physics **197**(1), 299–340 (2004)
31. Piller, M., Stalio, E.: Compact finite volume schemes on boundary-fitted grids. Journal of Computational Physics **227**(9), 4736–4762 (2008)
32. Pirozzoli, S.: Conservative hybrid compact-WENO schemes for shock-turbulence interaction. Journal of Computational Physics **178**(1), 81–117 (2002)
33. Ren, Y., Liu, M., Zhang, H.: A characteristic-wise hybrid compact-WENO scheme for solving hyperbolic conservation laws. Journal of Computational Physics **192**(2), 365–386 (2003)
34. Shen, Y., Yang, G., Gao, Z.: High-resolution finite compact difference schemes for hyperbolic conservation laws. Journal of Computational Physics **216**(1), 114–137 (2006)
35. Shu, C.: Essentially non-oscillatory and weighted essentially non-oscillatory schemes for hyperbolic conservation laws. Advanced numerical approximation of nonlinear hyperbolic equations pp. 325–432 (1998)
36. Shu, C.W., Osher, S.: Efficient implementation of essentially non-oscillatory shock-capturing schemes, ii. Journal of Computational Physics **83**(1), 32–78 (1989)
37. Sod, G.A.: A survey of several finite difference methods for systems of nonlinear hyperbolic conservation laws. Journal of Computational Physics **27**(1), 1–31 (1978)
38. Tao, T., Xu, K.: Gas-kinetic schemes for the compressible Euler equations: positivity-preserving analysis. Zeitschrift für angewandte Mathematik und Physik ZAMP **50**(2), 258–281 (1999)
39. Toro, E.F.: Riemann solvers and numerical methods for fluid dynamics: a practical introduction. Springer (2009)
40. Woodward, P., Colella, P.: The numerical simulation of two-dimensional fluid flow with strong shocks. Journal of Computational Physics **54**(1), 115–173 (1984)
41. Xiong, T., Qiu, J.M., Xu, Z.: Parametrized Positivity Preserving Flux Limiters for the High Order Finite Difference WENO Scheme Solving Compressible Euler Equations. submitted to Journal of Computational Physics
42. Zhang, S., Deng, X., Mao, M., Shu, C.: Improvement of convergence to steady state solutions of Euler equations with weighted compact nonlinear schemes. Acta Mathematicae Applicatae Sinica **29**, 449–464 (2013)
43. Zhang, S., Jiang, S., Shu, C.: Development of nonlinear weighted compact schemes with increasingly higher order accuracy. Journal of Computational Physics **227**(15), 7294–7321 (2008)
44. Zhang, X., Shu, C.: Maximum-principle-satisfying and positivity-preserving high-order schemes for conservation laws: survey and new developments. Proceedings of the Royal Society A: Mathematical, Physical and Engineering Science **467**(2134), 2752–2776 (2011)
45. Zhang, X., Shu, C.W.: On maximum-principle-satisfying high order schemes for scalar conservation laws. Journal of Computational Physics **229**(9), 3091–3120 (2010)
46. Zhang, X., Shu, C.W.: On positivity-preserving high order discontinuous galerkin schemes for compressible euler equations on rectangular meshes. Journal of Computational Physics **229**(23), 8918–8934 (2010)
47. Zhang, X., Shu, C.W.: Positivity-preserving high order discontinuous Galerkin schemes for compressible Euler equations with source terms. Journal of Computational Physics **230**(4), 1238–1248 (2011)
48. Zhang, X., Shu, C.W.: Positivity-preserving high order finite difference WENO schemes for compressible Euler equations. Journal of Computational Physics **231**(5), 2245–2258 (2012)

49. Zhang, X., Xia, Y., Shu, C.W.: Maximum-principle-satisfying and positivity-preserving high order discontinuous Galerkin schemes for conservation laws on triangular meshes. Journal of Scientific Computing **50**(1), 29–62 (2012)